Ultrathin, ordered oxide films on metal surfaces

2008 J. Phys.: Condens. Matter 20 264013

(http://iopscience.iop.org/0953-8984/20/26/264013)

J. Phys.: Condens. Matter **20** (2008) 264013 (11pp) doi:10.1088/0953-8984/20/26/264013

Ultrathin, ordered oxide films on metal surfaces

M S Chen[1,2] **and D W Goodman**[1]

[1] Department of Chemistry, Texas A&M University, PO Box 30012, College Station, TX 77842-3012, USA
[2] State Key Laboratory of Physical Chemistry for Solid Surface, Department of Chemistry, Xiamen University, Xiamen 361005, Fujian, People's Republic of China

Received 14 January 2008, in final form 4 April 2008
Published 9 June 2008
Online at stacks.iop.org/JPhysCM/20/264013

Abstract
Metal oxides and oxide thin films are extensively used as active catalysts and catalytic supports, as well as in many other important technical applications. Unlike TiO_2, which is a semiconductor and can be investigated using a variety of surface science techniques, most metal oxides are insulators, which seriously restricts their use as model surfaces with modern surface science techniques. This difficulty can be circumvented by synthesizing ultrathin oxide films a few nanometers in thickness with well-defined structures, that mimic the corresponding bulk oxides yet are thin enough to be sufficiently conducting. In this review, preparations, structures, electronic and chemical properties of four representative oxides, alumina, magnesium oxide, silica, and titania, are addressed. Of these MgO is found to grow in a layer-by-layer fashion, allowing preparation of crystalline thin film structures with varying thicknesses. Crystalline TiO_2 and Ti_2O_3 can also be synthesized, whereas SiO_2 and Al_2O_3, although amenable to synthesis as well-defined monolayer structures, have only been grown to date as amorphous multilayers.

(Some figures in this article are in colour only in the electronic version)

Acronyms used in the text

AES	Auger electron spectroscopy
AFM	Atomic force microscopy
ARUPS	Angle resolved ultraviolet photoelectron spectroscopy
DFT	Density function theory
EELS	Electron energy loss spectroscopy
ESR	Electron spin resonance
FTIRS	Fourier transform infrared spectroscopy
HREELS	High-resolution electron energy loss spectroscopy
IR	Infrared
LEED	Low energy electron diffraction
LEIS	Low energy ion scattering spectroscopy
MIES	Metastable impact electron spectroscopy
ML	Monolayers
NC-AFM	Non-contact atomic force microscopy
PM-RAIRS	Polarization modulation reflectance absorption infrared spectroscopy
RAIRS	Reflectance absorption infrared spectroscopy
SFVS	Sum-frequency vibrational spectroscopy
STM	Scanning-tunneling microscopy
STS	Scanning-tunneling spectroscopy
TDS	Thermal desorption spectrometry
TPD	Temperature programed desorption
UHV	Ultrahigh vacuum
XPD	X-ray photoelectron diffraction
XPS	X-ray photoelectron spectroscopy
XRD	X-ray diffraction

1. Introduction

Oxides are fundamentally important in heterogeneous catalysis as active catalysts and as supports for metal clusters, and many other important applications [1]. Many of the traditional techniques used to study heterogeneous catalysts are limited with respect to atomic-level characterization of metal supported catalysts. Work over the last two decades has demonstrated that atomic-level surface science techniques

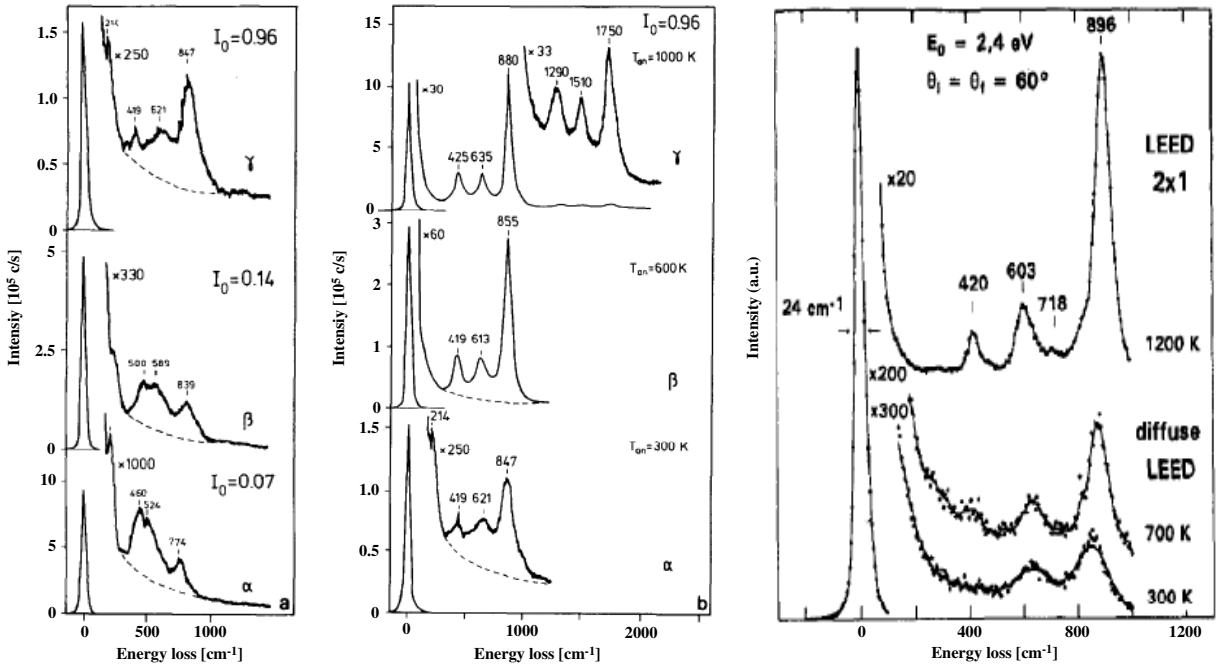

Figure 1. Left panel: HREEL spectra for increasing oxygen exposures up to 1200 L on NiAl(110) at room temperature; middle panel: HREEL spectra after a 1200 L O_2 exposure to NiAl(110) at room temperature following by an anneal at various temperatures; right panel: HREEL spectra after a 500 L O_2 exposure to NiAl(001) at room temperature following an anneal at various temperatures.

can provide fundamental insights into the physics and chemistry of oxide surfaces by the synthesis of ultrathin oxide films [2–20]. Deposition of metal clusters onto these oxide films allows complexities of oxide-supported metal catalysts to be addressed. These specially prepared model systems offer advantages typically found for single crystals, while addressing important issues of supported catalysts such as metal cluster size effects and the role of the oxide support. Representative oxide thin films have been shown to mimic the chemical and physical properties of the corresponding bulk oxides, yet are electrically conductive [11]. The conductivity and planarity of these model catalysts allow study with various charged particle spectroscopies that comprise the core of modern surface science while being suitable for study with scanning-tunneling microscopy. Here we focus on recent results of well-defined, thin oxide films. Results for four prototype oxide supports, alumina, magnesia, silica, and titania, are addressed.

2. Alumina thin films

Aluminum oxide (Al_2O_3) is thermodynamically the most stable compound of aluminum over a wide temperature range, and is a widely used support for heterogeneous catalysts. Ultrathin Al_2O_3 ordered layers on alloys are used as templates for model catalysts, tunneling barriers in electronic devices, and corrosion-resistant layers. An ultrathin, well-ordered alumina film of 4–5 Å in thickness can be grown by dosing oxygen with a subsequent anneal on low-index terminations of NiAl alloys such as NiAl(110) [21, 22] and Ni_3Al(111) [23–25].

Epitaxial growth of highly ordered Al_2O_3 films on NiAl(110) at temperatures between 620 and 670 K has been demonstrated using LEED, EELS, HREELS, XPS, ARUPS, and STM [21, 26–28]. NC-AFM [29, 30] reveals atomic rows with a 9 Å periodicity for the well-ordered Al_2O_3/NiAl(110). The stoichiometry of the O–Al bonds during oxygen absorption and realignment during annealing are found to be important in the epitaxial growth of well-ordered crystalline films [28]. Oxygen adsorption on NiAl(001) at room temperature reaches saturation quickly after an initial high sticking probability [31]. Figure 1 (left panel) shows a series of HREEL spectra for increasing oxygen exposure at room temperature on NiAl(110) [21]. The related Al–O phonon shifts from 774 to 847 cm^{-1} as a function of dosed oxygen up to saturation (1200 L). Annealing this oxygen saturated surface at 1000 K leads to a shift in the primary Al–O shifting to 880 cm^{-1} as shown in figure 1 (middle panel). Because an α-Al_2O_3 single crystal exhibits only two loss features at 496 and 806 cm^{-1} [32], a structural model similar to γ-Al_2O_3 was proposed. Four distinct loss features at 420, 603, 718 and 896 cm^{-1} were identified for Al_2O_3/NiAl(001) as shown in figure 1 (right panel) [31], very similar to spectra acquired from thin Al_2O_3 films grown on various substrates such as Al(111), NiAl(111) and Ru(0001). Group theory predicts six normal vibrational modes for an octahedral structure, with only two being infrared active. For the tetrahedral structure there are also two infrared active modes with four normal modes. In α-Al_2O_3, Al^{3+} ions occupy octahedral sites, resulting in two loss features at 496 and 816 cm^{-1} [32]. Thus, it was concluded that in Al_2O_3 thin films, the Al^{3+} ions occupy both octahedral and tetrahedral sites, as in θ-Al_2O_3 [31]. This conclusion is supported by XRD [33] and high-resolution soft XPS [34].

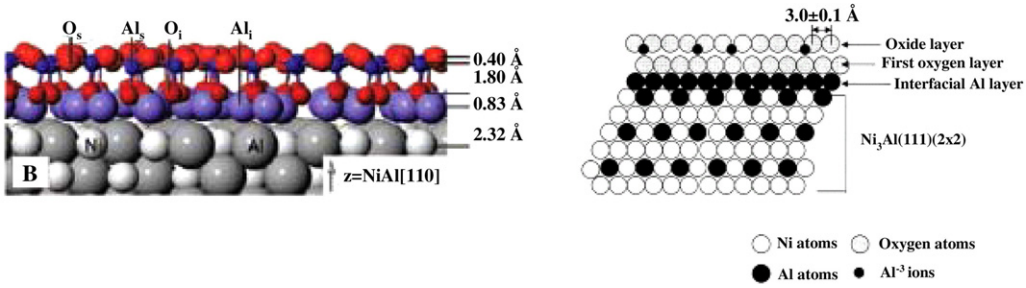

Figure 2. Structural models of ultrathin alumina films on (A) NiAl(110) and (B) $Ni_3Al(111)$.

Based on XRD [33] and high-resolution soft XPS [34] data, the highly ordered Al_2O_3/NiAl(110) thin film is proposed to consist of a double layer of strongly distorted hexagonal oxygen ions with aluminum ions in octahedral and tetrahedral sites (see figure 2). DFT calculations [35] support a model with an almost coplanar Al–O layer, as predicted for terminated bulk single crystal alumina surfaces. The film structure is characterized by Al ions in different coordinative environments, i.e. octahedral and tetrahedral, and compares with the structure believed to exist on an oxygen deficient corundum surface. The stoichiometry of the film is estimated to be $Al_{10}O_{13}$, i.e. an oxygen deficient alumina. The calculated phonon spectrum from this model agrees closely with those from experiment [35, 36]. It should be emphasized that there are two oxygen species in this ultrathin oxide film (see figure 2), one at the topmost surface, and one between Al^{3+} and the interface Al and/or Ni. The latter may resemble a species of incomplete oxidation of aluminum proposed by Yates and co-workers [37]. A key question is whether there should be two kinds of Al–O species with characteristic vibrational modes.

A smooth, continuous alumina film can also be grown on a $Ni_3Al(111)$ surface [23–25, 38, 39] with a thickness of one monolayer, comparable to that on NiAl(110) (see figure 2). A structure of the ultrathin aluminum oxide on $Ni_3Al(111)$ was determined to be $(\sqrt{67} \times \sqrt{67})R12.2°$ by a combination of STM and DFT. In addition to other local defects, the main structural feature of the unit cell is a 0.4 nm-diameter hole reaching to the metal substrate [40]. A remarkable feature of the ultrathin aluminum oxide film grown on $Ni_3Al(111)$ is its surface reconstruction resulting in a dot structure with a large rhombic surface unit cell. Besides this, 5%–20% of the surface area may be covered by another reconstruction that is characterized by zigzag features arranged in parallel stripes. Both phases consist of a modulated hexagonal lattice with 0.51 nm periodicity resembling the aluminum sub-lattice of the $Ni_3Al(111)$ substrate [41]. Al_2O_3 films of 7 Å thickness grown on both $Ni_3Al(110)$ and $Ni_3Al(111)$, undergo severe reconstruction and loss of long-range order upon exposure to H_2O at pressures above 10^{-5} Torr at 300 K. The reconstruction process begins at the oxide surface, not the oxide/metal interface, and is not associated with formation of a UHV-stable hydroxide phase [42]. This surface serves as an ideal nano-template for metal nano-particles [43]. The heteroepitaxial growth of thin $Al_2O_3(111)$ films on Ta(110) has been studied using LEIS and LEED and the initial film growth found to be largely 2D clusters [44]. The LEED results indicate formation of a long-range, ordered epitaxial Al_2O_3 film with a slightly distorted ($\beta = 117.9°$) hexagonal lattice. Detailed structural analysis has shown that the hexagonal lattice is due to an ordered, close-packed oxygen anion layer associated with either the (0001) face of α-Al_2O_3 or the (111) face of α-Al_2O_3. Chemically, the $Al_2O_3(111)$/Ta(110) film is very inert towards a variety of gas molecules, indicating no unsaturated surface bonds. Highly ordered and stoichiometric thin Al_2O_3 films with various thicknesses have also been prepared on a Mo(110) [45], Mo(100) [46] and Ru(0001) [47].

3. Magnesium oxide thin films

Magnesium oxide (MgO) is an ionic oxide of a rock-salt structure with alternation of ions with opposite charges [48]. MgO is often chosen as representative of metal oxides, due to its simple bulk and (100) surface structures. The (100) surface is stable, irreducible, nonpolar, and easy to prepare with well-defined stoichiometry [49–51]. Oxygen vacancies leave electrons trapped in the vacancy, i.e. a pair or a single electron as F or F^+ centers, respectively. The oxygen vacancies are of great importance in defining the overall properties and chemical reactivity of MgO [52–55]. Well-ordered surfaces of MgO with low-defect density can be created by cleaving bulk single crystals. MgO is one of the most commonly used catalyst supports and is used in semiconductor devices as a high-k dielectric [56]. MgO(100) films have been prepared mainly on Mo(100) and Ag(100) substrates. Epitaxial MgO(100) with a thicknesses ranging from 2 to 100 ML can be grown by evaporating Mg onto Mo(100) at 300 K in 10^{-6} Torr of oxygen [57–67]. LEED indicates the growth of MgO(100) films with the MgO(110) oriented along the ⟨100⟩ direction of the Mo(001) substrate [68–70]. Despite the insulating nature of bulk MgO, films up to 15 ML thick have been imaged by STM [71, 72]. The films, stable up to 1300 K, are reduced at higher temperatures by the Mo substrate, forming MoO_x and Mg vapor. The electronic and vibrational structure of thin MgO films (see figure 3) are very similar to those of the bulk oxide [73–80]. The main difference between the thin films and bulk MgO(001) is the higher defect density in the former compared to the latter [81].

MgO(100)/Ag(100) systems have been prepared by evaporating metallic Mg from an alumina crucible in an oxygen background of 5×10^{-7} Torr at 350 K followed

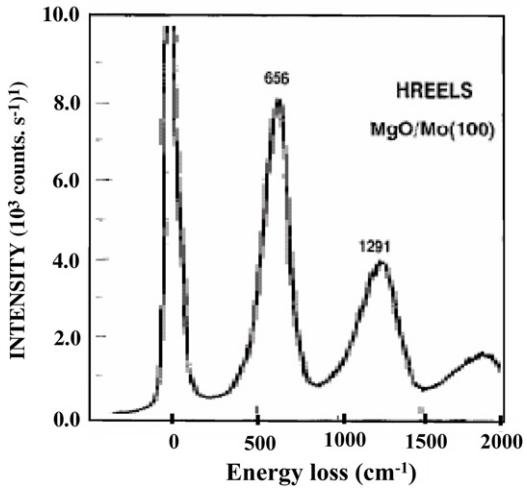

Figure 3. HREEL spectrum obtained from a 10 ML MgO film on Mo(100); beam energy is 2 eV.

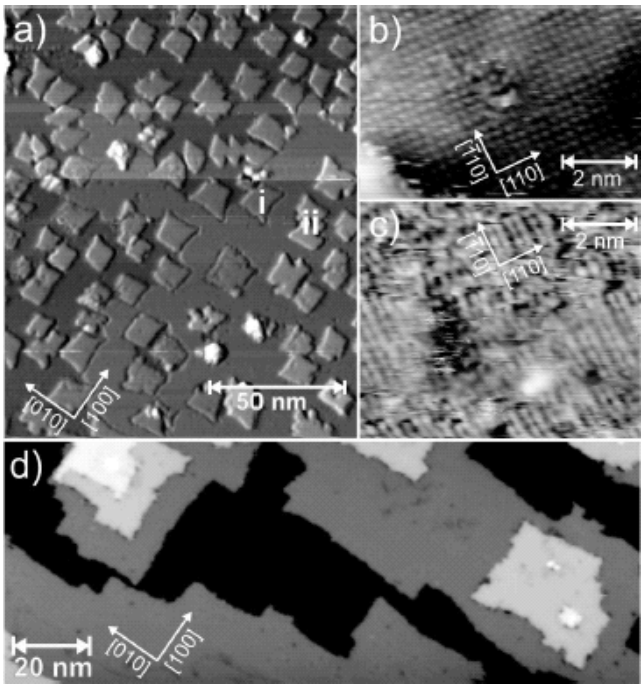

Figure 4. STM images of (a) 0.3 ML MgO/Ag(001), $U = 5.0$ V, $I = 1.0$ nA; (b) Ag(001) atomic resolution through an MgO island, $U = 30$ mV, $I = 2$ pA; (c) atomic resolution of the MgO layer (one type of ion is resolved) $U = 2.5$ V, $I = 50$ pA; (d) 2.0 ML MgO/Ag(001), $U = 3.0$ V, $I = 1.0$ nA.

by annealing to 500 K [82–93]. As in the case of MgO(100)/Mo(100) [50, 57–61, 94–98] the as-prepared film appears to be free of point defects (color centers). Upon irradiation with electrons, color centers can be produced and detected by EELS. Exposure to oxygen quenches these defects indicating their presence within the surface layer. Low-temperature STM has been used to image the growth of the MgO(100) film on Ag(100) and the creation of color centers [84, 85, 88]; a series of images is shown in figure 4. MgO initially forms two-dimensional square islands homogeneously distributed on the surface. At 1 ML, approximately 60% of the substrate surface is covered by 2D domains. At MgO coverages of 2–3 ML, the surface is completely covered, with a typical terrace size of ∼20 nm. Layer-resolved differential conductance (dI/dU) measurements show that a three monolayer film has a band gap of ∼6 eV, comparable to a MgO(001) single crystal. Layer-resolved DFT calculations corroborate this finding [88]. This MgO film exhibits line defects by LEED profile analysis; point defects only become apparent via STS after electron bombardment; these paramagnetic surface colors centers have been detected using ESR spectroscopy [84]. These results can be directly compared with studies on powder samples [99–101]. On mono- and bilayer domains of MgO/Ag(001), the edges are mainly oriented along the ⟨110⟩ oxide direction, corresponding to polar perimeters, while on multilayer domains nonpolar perimeters appear, corresponding to the ⟨100⟩ orientation [102].

Thin MgO films (1–20 ML) synthesized by evaporating metallic Mg in an oxygen atmosphere onto Ag(100) exhibit a relative small lattice misfit (3.1%) between the (100) surface of fcc Ag and the MgO rock-salt structure. This lattice match facilitates epitaxial growth of MgO layers with (001)MgO parallel to (001)Ag and (100)MgO parallel to (100)Ag [87]. In spite of the weak interaction between the oxide overlayer and the substrate, there is significant tetragonal distortion of the MgO structure. At a substrate temperature of 450 K, a single-domain MgO film ([100] (film) ∥ [100] (substrate)) grows heteroepitaxially on Ag(100) [103]. The in-plane lattice constant of the film changes continuously from the substrate value to that of the film. MgO adsorbs preferentially with the oxygen atom over the Ag atom and the Mg atom over the hollow site. The lattice constant increases gradually from bulk Ag(100) to that of bulk MgO(100). The lattice constant of the film is nearly equal to that of bulk MgO for films thicker than 20 ML.

The local atomic structure of MgO epitaxial layers on Ag(100) has been determined by polarization-dependent XAS at the Mg(K) and O(K) edges [104]. At the ultrathin limit, the local structure of the films is rock salt. An in-plane compressive strain, due to lattice mismatch with the Ag substrate, is present for the 3 ML film. The out-of-plane lattice constant is found to expand, in agreement with the expected behavior for a tetragonal distortion of the unit cell. This growth-induced strain is gradually released with increasing thickness and is almost completely relaxed at 20 ML. Any significant intermixing with the Ag substrate has been ruled out.

Figure 5 shows vibrational spectra for MgO films on Ag(100) as a function of MgO thickness [105]. Several features are present in the range between 400 and 700 cm^{-1}, with the position and intensity strongly dependent on film thickness. A phonon feature maximum at ∼524 cm^{-1} appears for each film shifting little with thickness. The phonon at 572–677 cm^{-1} appears after the growth of the second layer, with a significant intensity increase and a blue shift in peak position. For a thicker MgO film on Mo(100), a single phonon at 656 cm^{-1} was observed. No specific vibrational modes

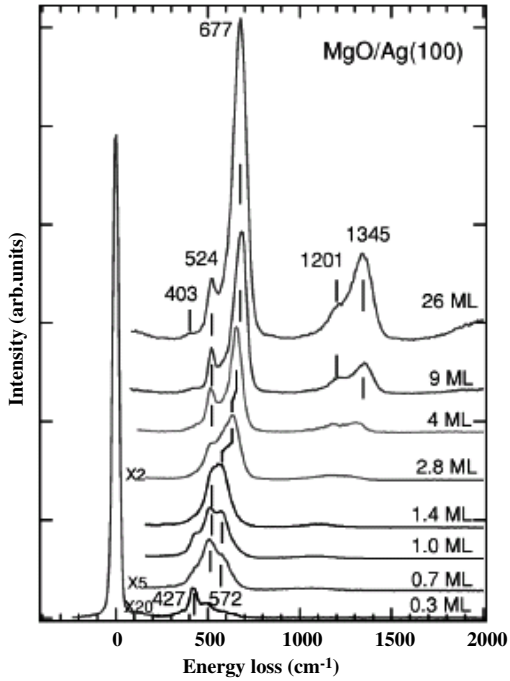

Figure 5. HREEL spectra of MgO films of various thicknesses on Ag(100). $E_p = 4.0$ eV, except for the two upper ones where $E_p = 3.0$ eV. Note that the second layer appears at a coverage below 0.6 ML by STM.

were assigned in [105]; however, various arrangements of the oxygen species, i.e. Mg–O–Ag and Mg–O–Mg, are likely at the ultrathin limit.

The growth of epitaxial and stoichiometric MgO(111) thin films on a Mo(110) surface has been demonstrated using LEED, XPS, AES, and LEIS [106, 107]. The MgO(111)/Mo(110) film is stable up to 1400 K, and is reduced by the Mo substrate at higher temperature, forming MoO_3 and Mg vapor. By alternating the deposition of Mg and O_2, layer-by-layer growth of polar MgO(111) ultrathin films with Mg-terminated or O-terminated surfaces has been successfully carried out on a Mo(110) substrate [108]. The geometric structure of MgO deposited on Fe(001) in UHV was determined in detail using XRD [109]. In contrast to the common belief that MgO grows in direct contact to the Fe(001) substrate, a FeO interface layer between the substrate and the growing MgO structure was proposed. MgO films with a thickness of 2 nm have been reported to grow on W(110) [110].

4. Silica thin films

Silica (SiO_2) is an important support material used in many commercial catalyst systems [1]. Thin amorphous SiO_2 films have been synthesized on Mo(110) and Mo(100) substrates [16, 111–113] by evaporating silicon onto the respective substrate at room temperature in $< \sim 2 \times 10^{-5}$ Torr O_2 background followed by an anneal at $< \sim 1300$ K. The as-prepared film is predominantly silicon dioxide with a small fraction of suboxides (SiO) as indicated by AES, XPS and RAIRS. Annealing to approximately 1300 K yields a stoichiometric film of SiO_2. The suboxides are believed to react further with oxygen to form SiO_2 at elevated temperatures. The silicon oxide films prepared at room temperature exhibit additional low energy electron loss features at ∼5 and 7 eV. These features are attributed to a local structure with broken Si–O bonds in tetrahedra of (SiO_4) and the presence of some suboxide. After annealing at ∼1200 K, these features disappear, yielding EELS features essentially identical to those of vitreous silica. These results are consistent with the formation of low-defect vitreous silica consisting of (SiO_4) tetrahedra connected by an oxygen bridge to form a long-range 3D network. RAIRS (see figure 6) further illustrates that such structural changes occur when the silicon dioxide films are annealed. The asymmetric stretching mode of the Si–O bonds appears as a broad asymmetric peak centered at 1178 cm^{-1} in the RAIRS spectrum for the film prepared at a substrate temperature of 323 K. This peak gradually shifts to higher frequency upon heating and reaches a maximum of 1252 cm^{-1} as the silicon dioxide film is annealed to $> \sim 1300$ K. Furthermore, the line shapes, the peak energies of the AES electrons, and the EELS spectra are consistent with those of silicon dioxide. The SiO_2 films are thermally stable up to 1600 K with the stability increasing with film thickness. At high temperatures, silicon dioxide is reduced by the Mo substrate to form volatile SiO and MoO_3.

Ordered silica films have been grown on Mo(112) [114–117]. This film, which exhibits a sharp $c(2 \times 2)$ LEED pattern, was shown to have a thickness of 1 ML as estimated from AES intensity attenuation of the Mo(MNN) feature (187 eV) and to exhibit self-limited growth properties [118–120]. The orientation and growth of benzene and pyridine were used to characterize the quality of the SiO_2 films via HREELS, AES and LEED [121]. A single vibrational mode corresponding to the Si–O asymmetric vibration was observed at ∼1050 cm^{-1} as indicated in figure 6, which is significantly lower than that of ∼1180 cm^{-1} observed for a thicker SiO_2 films or single crystal. Regarding the fact that the film thickness is 1 ML, this mode at ∼1050 cm^{-1} was assigned to the asymmetric vibration of Si–O–Mo [118]. The absence of the mode for the asymmetric vibration of Si–O–Si for this ultra thin film led to the conclusion that the film thickness was no greater than 1 ML, and to the conclusion that the structure consists of isolated (SiO_4) units as shown in figure 7 (A) [118], a conclusion supported by DFT calculations [122]. In contrast a 2D network of SiO_4 tetrahedra where one oxygen is bound to the metal substrate and the other three form a hexagonal honeycomb structure (see figure 7(B)) has been proposed [123–127]. This 2D network model in fact contradicts experimental results [118, 121, 128]. The axis of the Si–O–Si in the 2D network model is proposed to be parallel with the surface, thus the asymmetric vibrational mode of Si–O–Si should be infrared inactive, yet is absent in IRAS and on-specular HREEL spectra. Also off-specular HREEL shows no feature at ∼1176 cm^{-1} characteristic of the asymmetric vibration of Si–O–Si (figure 8). Furthermore the bending mode of Si–O–Si in the proposed 2D network model lies perpendicular to the surface, i.e. infrared active, yet is not observed in HREEL data (see figure 6) [118, 128]. The DFT

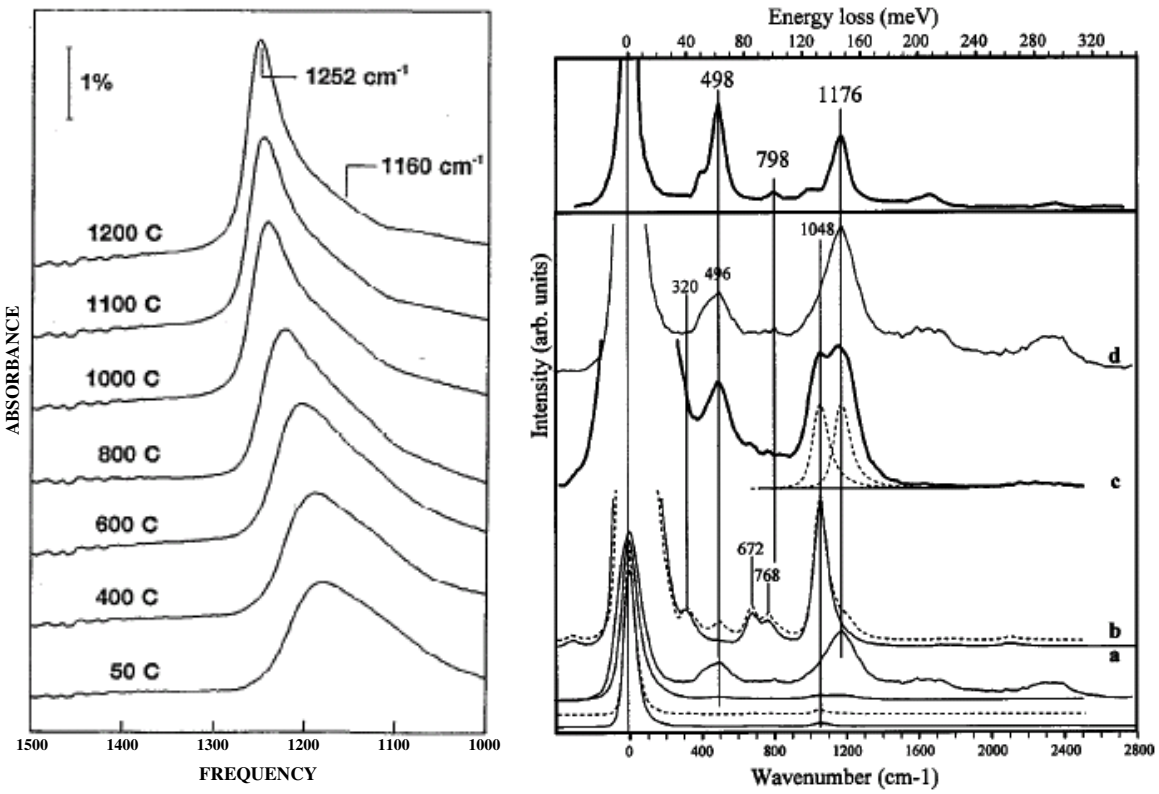

Figure 6. Left panel: infrared reflection absorption spectra for a ∼5 nm silicon dioxide film on a Mo(110) annealed at various temperatures. Right panel: HREEL spectra of SiO_2 films on Mo(112) at various coverages. (a) 1 ML (solid line), (b) ∼1.2 ML (dotted line), (c) ∼1.8 ML, (d) ∼5 ML, and (top) from quartz(0001). The bottom four lines show the full spectra for (a)–(d).

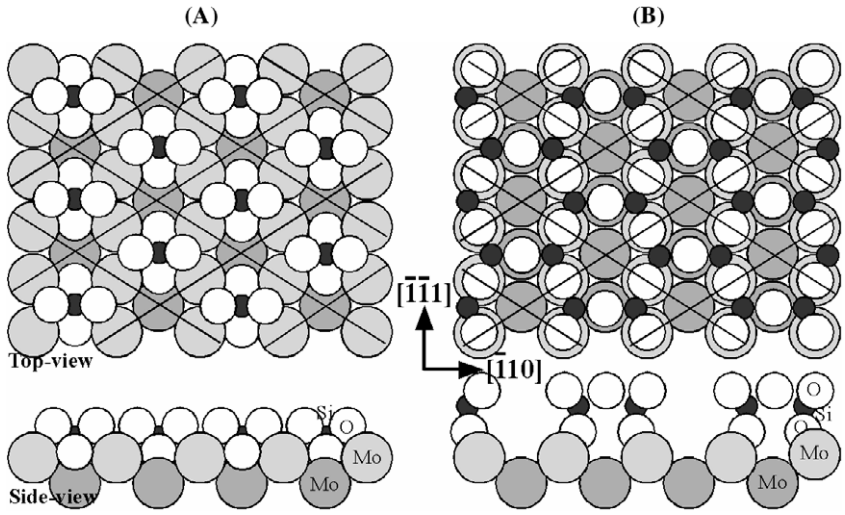

Figure 7. Top- and side-view of the structural models of (A) isolated (SiO_4). and (B) 2D network for SiO_2 (1 ML)/Mo(112).

calculations in [123–125] are used to support the 2D network model, however, these calculation more consistently support the isolated (SiO_4) structural model as discussed in [128] and shown in figure 9. Furthermore, detailed atomically resolved STM features as shown in figures 10 and 11 support the isolated (SiO_4) model and are inconsistent with the 2D network model [120]. More recently, Kaya *et al* [132] have provided more experimental detail and summarized most of the related literature data in favor of the 2D network model. Unfortunately, Kaya *et al* [132] neglected to discuss an important piece of experimental information, i.e. the absence of an asymmetrical Si–O–Si vibrational mode in the off-specular HREELS spectrum as well as the absence of a Si–O–Si bending mode in the HREELS spectrum [120, 128]. The absence of these modes is strong evidence against the 2D network model. Furthermore, the arguments used by Kaya *et al* in favor of the 2D network model essentially ignore the detailed atomically resolved STM data of Chen *et al* [120] that

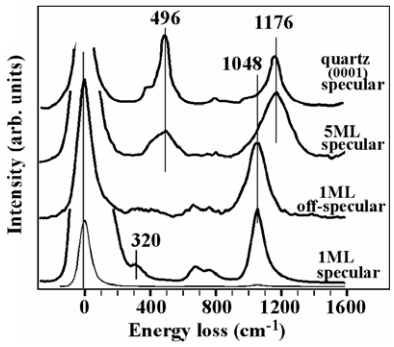

Figure 8. Comparison of HREEL spectra of SiO_2 films on Mo(112) at coverages of 1 and 5 ML, and from quartz(0001), with an off-specular spectrum of 1 ML SiO_2/Mo(112).

are entirely inconsistent with the 2D network model. Therefore the detailed structure of monolayer SiO_2/Mo(112) is still an issue yet to be resolved.

H_2O molecularly adsorbs on low- and high-defect SiO_2/Mo(112), forming 3D water clusters even at low coverage. No evidence for dissociation of water was found [133, 134]. Various defect sites on SiO_2/Mo(112) have been characterized with MIES and UPS [80, 135, 136].

5. Titania thin films

Titanium dioxide (TiO_2) is the most thoroughly single-crystalline oxide investigated by surface science techniques, owing to its semiconducting properties. Rutile (110), (100), (001), and anatase surfaces have been studied. Among them, rutile (110) has been studied most extensively. Since TiO_2 is important for a wide range of technical uses, the bulk structure, defects, and electronic structure have been extensively studied and summarized [137]. A high-resolution STM image and schematic structural model of TiO_2(110) are shown in figure 12 [138].

Ultrathin (<10.0 nm) titanium oxide films can be synthesized on a Mo(100) surface [139]. Epitaxial growth with varying film thickness studied by LEIS, XPS, AES, and LEED show a $(2\sqrt{2} \times \sqrt{2})$R45 diffraction pattern whereas STM images indicate that the TiO_2 films are ordered along the [010] and [001] directions of the Mo(100) substrate. XPS data reveals that unannealed titanium oxide films exhibit only a Ti^{4+} valence state, whereas annealed titanium oxide films are partially reduced and exhibit Ti^{3+} and Ti^{2+} states. Ordered titanium oxide films can also be epitaxially grown on a Mo(110) substrate [140, 141]. Using various synthetic methods, TiO_2(100) or Ti_2O_3(0001) have been synthesized, as evidenced by (1 × 1) rectangular and (1 × 1) hexagonal LEED patterns, respectively, with supporting data from AES and XPS. STM indicates layer-by-layer growth at 900 K with the presence of flat terraces with three different orientations. The spacings between the neighboring atomic rows for all terraces were similar (0.65 nm), suggesting epitaxial growth of TiO_2(110)-(1 × 1). TiO_2 films have also been grown on Ni(110) [142, 143] and W(100) [144].

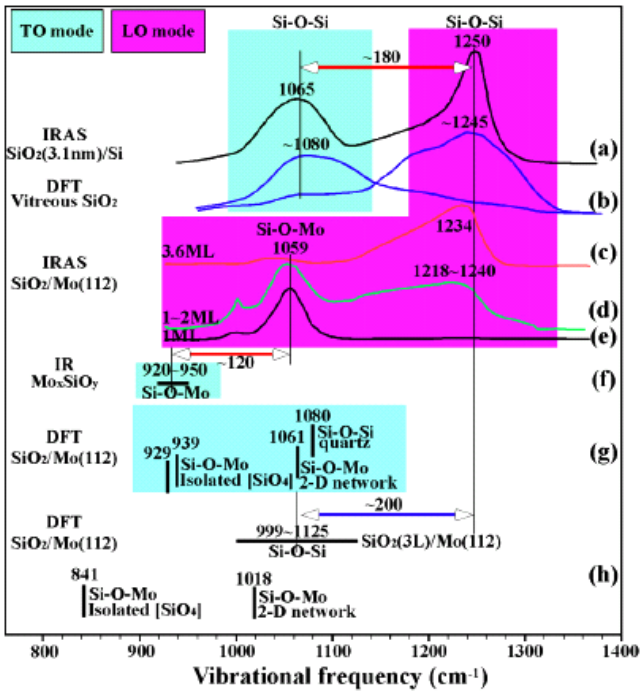

Figure 9. Frequency of the asymmetric Si–O vibrational mode: (a) thermally grown SiO_2 (3.1 nm)/Si using IRAS at a glazing angle of 22° [129]; (b) DFT of vitreous SiO_2 [130]; (c)–(e) SiO_2/Mo(112) with a thickness of 1, 1.2 and 3.6 ML, respectively, using IRAS at a glazing angle of 84° [117, 119]; (f) Mo_xSiO_y using transmission IR [131]; (g) DFT obtained TO modes of SiO_2 (1 ML) by Todorova *et al* [124, 125] and (h) DFT obtained TO modes of SiO_2/Mo(112) by Giordano *et al* [123].

Titanium oxide thin films can also be grown on Pt(111) by vapor phase deposition of titanium metal followed by oxidation in 10^{-6} Torr O_2 [145, 146]. A three-fold symmetric structure with a unit cell of 1.82 × 1.82 nm is observed at coverages ranging from 1.0 to 5.0 ML. XPS measurements of this phase show stoichiometric TiO_2. Heating in vacuum at 650–850 °C leads to a new structure with a unit cell of 1.82 × 1.39 nm which is shown by XPS to have the stoichiometry of Ti_4O_7. Angle resolved XPS measurements indicate that reduced Ti^{3+} is concentrated at the oxide/Pt(111) interface. By varying the Ti coverage and the annealing conditions, six different long-range ordered phases of TiO_x are obtained. XPS binding energy and XPD data indicate that all the phases, except one (the stoichiometric rect-TiO_2), are one monolayer thick and composed of a Ti-O bilayer with interfacial Ti. Atomically resolved STM images confirm that these TiO_x phases wet the Pt surface, in contrast to rect-TiO_2.

Surface structures formed by titanium oxide thin films at a Pt(100) surface have been studied by STM, LEED, AES, XPS, XRD and LEIS to explore and elucidate stable high-temperature structures that form at titania–Pt interfaces and provide a basis for characterizing the chemistry of titania thin films on Pt(100) [147]. Titanium oxide films were produced by two different methods, the first via oxidation of a Pt_3Ti surface alloy at 300 K using ozone (O_3) and annealing at 1000 K. Smooth thin films with a (3 × 5) structure were observed at 1 ML (monolayer) using this procedure. This (3 × 5) structure

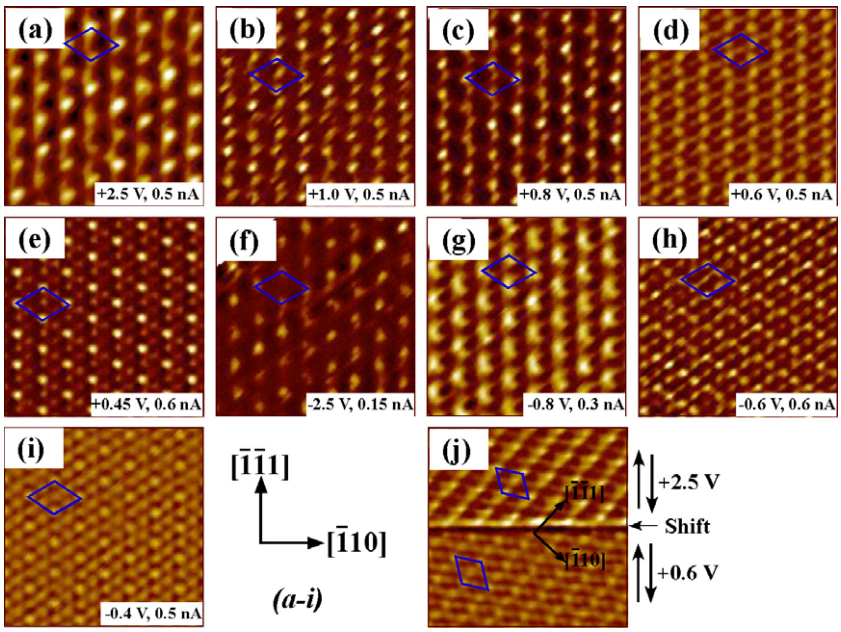

Figure 10. STM images of SiO_2 (1 ML)/Mo(112) at various sample bias voltages. All images are 3.5 nm × 3.5 nm. (a) $U_S = +2.5$ V, $I = 0.5$ nA; (b) $U_S = +1.0$ V, $I = 0.5$ nA; (c) $U_S = +0.8$ V, $I = 0.5$ nA; (d) $U_S = +0.6$ V, $I = 0.5$ nA; (e) $U_S = +0.45$ V, $I = 0.6$ nA; (f) $U_S = -2.5$ V, $I = 0.15$ nA; (g) $U_S = -0.8$ V, $I = 0.3$ nA; (h) $U_S = -0.6$ V, $I = 0.6$ nA; (i) $U_S = -0.4$ V, $I = 0.5$ nA. (j) and (k) the bias voltage was shifted from +0.6 to +2.5 V mid-way during the upward scan and shifted back from +2.5 to +0.6 V during the downward scan to complete the scan as indicated in the figure. Lower panel: $U_S = +0.6$ V, $I = 0.5$ nA; upper panel: $U_S = +2.5$ V, $I = 0.5$ nA. The $c(2 \times 2)$ unit is indicated in each image.

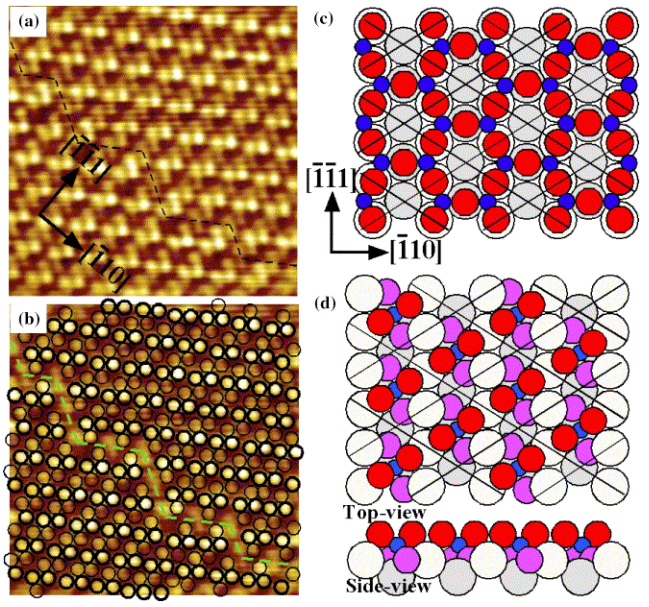

Figure 11. (a) STM image of SiO_2 (1 ML)/Mo(112) at $U_S = -3.0$ V, $I = 0.3$ nA. The image size is 5.5 nm × 5.5 nm. (b) Image A superimposed with thick and thin circles showing the oxygen atoms in the topmost layer and in the Mo(112) troughs in the isolated (SiO_4) model. (c) Top-view of the structural model of the 2D network highlighting the surface Si and oxygen atoms. (d) Top- and side-view of the modified structural model of isolated (SiO_4) for SiO_2 (1 ML)/Mo(112).

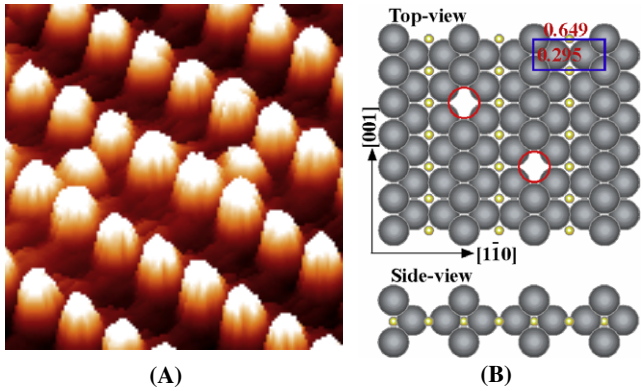

Figure 12. (A) A high-resolution STM image of TiO_2(110), (B) a schematic structural model of TiO_2(110) with empty circles indicating the surface oxygen vacancies.

is a monolayer Ti_2O_3 film that is similar to the (1 × 2) strands formed on reduced TiO_2(110) surfaces. Structures prepared by this method show particularly 'flat' terraces without islands. A second method of synthesis is by Ti evaporation and deposition on Pt(100) in 6.7 × 10^{-5} Pa O_2 followed by an anneal above 750 K in vacuum. A (3 × 5) structure was also produced for these films below 1 ML. A (4 × 3$\sqrt{5}$)R60° structure was observed after deposition of 2 ML and annealing at 850–1000 K. A model for this structure composed of TiO_2 tetragonal nets with a fraction of the O atoms in the second layer was proposed. The (4 × 3$\sqrt{5}$)R60° film changes to a (3 × 5) structure after annealing above 960 K in vacuum. TiO_2 clusters decompose to form a (2$\sqrt{2}$ × 2$\sqrt{2}$)R45° structure, proposed to be Ti_5O_8, and (3 × 5) domains after annealing at 1300 K. Based on this model, the composition of all titanium oxide ultrathin films on a Pt(100) surface is $TiO_{2\sim1.5}$

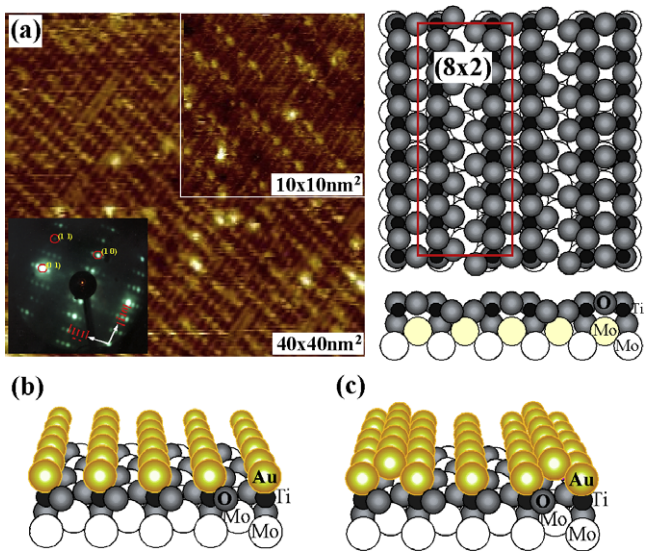

Figure 13. Structural model and atomic resolved STM image of (a) Mo(112)-(8 × 2)-TiO_x, (b) Mo(112)-(1 × 1)-(Au,TiO_x) and (c) Mo(112)-(1 × 3)-(Au, TiO_x).

after annealing at 850–1300 K. Chemical changes occurring during annealing of titanium oxide films include Ti dissolution (alloying) into the bulk of the Pt(100) crystal. Oxidation of the (3 × 5)-Ti_2O_3 film using O_3 or NO_2 (nitrogen dioxide) at 600 K and subsequent annealing to 700–950 K in vacuum produces ordered oxide regions and domains of a (4 × 13) structure that are attributed to a TiO_2 film with a square –Ti–O– net. The (4 × 13) film transforms to $(2\sqrt{2} \times 2\sqrt{2})$R45°-$Ti_5O_8$ domains after annealing at a higher temperatures between 1000 and 1100 K, and decomposes to the (3 × 5)-Ti_2O_3 oxide film with further annealing at 1200 K. Initial oxidation of a 'flat' (3 × 5) oxide film at 600 K reconstructs this surface to form a multilayer, porous oxide film. More extensive oxidation eventually forms a much less porous oxide film with pyramidal oxide crystallites. The titanium oxide films on Pt(100) described above block adsorption of CO at Pt sites at temperatures above 210 K; these surfaces also do not oxidize CO.

A well-ordered monolayer titanium oxide film, Mo(112)-(8 × 2)-TiO_x, can be synthesized on the Mo(112) surface [148–150]. A TiO_x/Mo(112) film was synthesized by depositing ∼1 ML Ti onto a SiO_2(ML)/Mo(112) followed by oxidation/annealing. A final anneal at 1400 K completely removes the SiO_2 film and any residual Si. The TiO_x film so formed exhibits a very sharp (8 × 2) LEED pattern (insert of figure 13(a)) and a very smooth, well-ordered surface with relatively large terraces apparent by STM (figure 13(a)). The thickness of this TiO_x film is estimated to be one monolayer based on the attenuation of the AES intensity of the Mo MNN (187 eV) feature. The (8 × 2)-TiO_x film can also be synthesized by the step-wise deposition of Ti onto an oxygen-covered Mo(112) surface followed by oxidation–annealing cycles. However, the quality and reproducibility of the TiO_x film derived from the direct deposition method indicate this method to be inferior to a film grown on SiO_2. A single phonon feature at 84 meV, related to the Ti–O stretching mode, was observed for the (8 × 2) structure. This feature was assigned to Ti^{3+}–O–Mo and/or Ti^{3+}–O–Ti^{3+} based on HREELS and XPS data [148–150]. A row spacing of 0.9 nm, corresponding to two rows of the Mo(112) trough along the [$\bar{1}$10] direction, is seen by STM (figure 13(a)), consistent with the observed (8×2) LEED pattern. High-resolution STM shows a double-row feature with a spacing of 0.9 nm. A proposed structural model for the Mo(112)-(8 × 2)-TiO_x surface is shown in figure 13 in which seven Ti atoms decorate every eight Mo atoms along the Mo(112) trough (the [$\bar{1}\bar{1}$1] direction). The Ti atoms are bound to the surface via Ti–O–Mo bonds and to each other via Ti–O–Ti linkages [148, 149]. This is the first oxide support that Au completely wets forming well-ordered gold mono- and bilayer films, as shown in figures 13(b) and (c) [148, 151–155].

6. Conclusions

An abundance of recent studies has demonstrated the synthesis of a large family of ultrathin oxide films. These thin films are electronic conductive, which enable their exploration using a variety of surface techniques, and thus offer unprecedented opportunities to address the details of the structure, electronic properties, and chemistry of metal oxides at the atomic/molecular level. These thin films as model oxide supports provide a convenient method to study important aspects of supported metal catalysts such as cluster size effects, cluster morphology, and support–cluster interactions, and allow bridging of the pressure and material gaps of catalysis using operando techniques such as RAIRS, SFVS, etc.

Acknowledgments

We acknowledge with pleasure the financial support of this work by the Department of Energy, Office of Basic Energy, Division of Chemical Sciences, and the Robert A Welch Foundation.

References

[1] Ertl G, Knözinger H and Weikamp J T (ed) 1997 *Handbook of Heterogeneous Catalysis* (Weinheim: Wiley–VCH)
[2] Freund H-J, Kuhlenbeck H and Neumann M 1993 *Adsorption on Ordered Surfaces of Ionic Solids and Thin Films* vol 33, ed E Umbach and H-J Freund (Heidelberg: Springer) p 136
[3] Henrich V E and Cox P A 1994 *The Surface Science of Metal Oxides* (Cambridge: Cambridge University Press)
[4] Goodman D W 1995 *Chem. Rev.* **95** 523
[5] Freund H-J, Kuhlenbeck H and Staemmler V 1996 *Rep. Prog. Phys.* **59** 283
[6] Campbell C T 1996 *J. Chem. Soc. Faraday Trans.* **92** 1435
[7] Goodman D W 1996 *J. Phys. Chem.* **100** 13090
[8] Campbell C T 1997 *Surf. Sci. Rep.* **27** 1
[9] Gunter P L J, Niemantsverdriet J W, Ribeiro F H and Somorjai G A 1997 *Catal. Rev. Sci. Eng.* **39** 77
[10] Henry C R 1998 *Surf. Sci. Rep* **31** 235
[11] Rainer D R and Goodman D W 1998 *J. Mol. Catal.* A **131** 259
[12] Chambers S A 2000 *Surf. Sci. Rep.* **39** 105
[13] Franchy R 2000 *Surf. Sci. Rep.* **38** 195
[14] Campbell C T, Grant A W, Starr D E, Parker S C and Bondzie V A 2001 *Top. Catal.* **14** 43

[15] Goodman D W 1995 *Surf. Rev. Lett.* **2** 9
[16] Goodman D W 1996 *J. Vac. Sci. Technol.* A **14** 1526
[17] Freund H-J 1997 *Angew. Chem. Int. Edn Engl.* **36** 452
[18] Heiz U and Landman U 2007 *Nanocatalysis* (Berlin: Springer)
[19] Yoon B, Landman U, Wörz A, Antonietti J-M, Abbet S, Judai K and Heiz U 2005 *Science* **307** 403
[20] Freund H-J 2007 *Surf. Sci.* **601** 1438
[21] Jaeger R M, Kuhlenbeck H, Freund H-J, Wuttig M, Hoffmann W, Franchy R and Ibach H 1991 *Surf. Sci.* **259** 235
[22] Libuda J, Winkelmann F, Bäumer M, Freund H-J, Bertrams T, Neddermeyer H and Müller K 1994 *Surf. Sci.* **318** 61
[23] Becker C, Kandler J, Raaf H, Linke R, Pelster T, Dräger M, Tanemura M and Wandelt K 1998 *J. Vac. Sci. Technol.* A **16** 1000
[24] Rosenhahn A, Schneider J, Becker C and Wandelt K 2000 *J. Vac. Sci. Technol.* A **18** 1923
[25] Rosenhahn A, Schneider J, Kandler J, Becker C and Wandelt K 1999 *Surf. Sci.* **433–435** 705
[26] Bäumer M and Freund H-J 1999 *Prog. Surf. Sci.* **61** 127
[27] Kulawik M, Nilius N, Rust H-P and Freund H-J 2003 *Phys. Rev. Lett.* **91** 256101
[28] Lay T T, Yoshitake M and Mebarki B 2002 *J. Vac. Sci. Technol.* A **20** 2027
[29] Pang C L, Raza H, Haycock S A and Thornton G 2002 *Phys. Rev.* B **65** 201401
[30] Hamm G, Barth C, Becker C, Wandelt K and Henry C R 2006 *Phys. Rev. Lett.* **97** 126106
[31] Gassmann P, Franchy R and Ibach H 1993 *J. Electron Spectrosc. Relat. Phenom.* **64-65** 315
[32] Liehr M, Thiry P A, Pireaux J J and Caudano R 1984 *J. Vac. Sci. Technol.* A **2** 1079
[33] Stierle A, Renner F, Streitel R, Dosch H, Drube W and Cowie B C 2004 *Science* **303** 1652
[34] Mulligan A, Dhanak V and Kadodwala M 2005 *Langmuir* **21** 8312
[35] Kresse G, Schmid M, Napetschnig E, Shishkin M, Köhler L and Varga P 2005 *Science* **308** 1440
[36] Frank M, Wolter K, Magg N, Heemeier M, Kuhnemuth R, Baumer M and Freund H J 2001 *Surf. Sci.* **492** 270
[37] Chen P J, Colaianni M L and Yates J T Jr 1990 *Phys. Rev.* B **41** 8025
[38] Kurnosikov O, Flipse C F J, Swagten H J M, Koopmans B and De Jonge W J M 2006 *Japan. J. Appl. Phys.* I **45** 2215
[39] Degen S, Krupski A, Kraj M, Langner A, Becker C, Sokolowski M and Wandelt K 2005 *Surf. Sci.* **576** L57
[40] Schmid M, Kresse G, Buchsbaum A, Napetschnig E, Gritschneder S, Reichling M and Varga P 2007 *Phys. Rev. Lett.* **99** 196104
[41] Gritschneder S, Degen S, Becker C, Wandelt K and Reichling M 2007 *Phys. Rev.* B **76** 014123
[42] Qin F, Magtoto N P and Kelber J A 2004 *Surf. Sci.* **565** L277
[43] Becker C, Rosenhahn A, Wiltner A, Von Bergmann K, Schneider J, Pervan P, Milun M, Kralj M and Wandelt K 2002 *New J. Phys.* **4** 75
[44] Chen P J and Goodman D W 1994 *Surf. Sci.* **312** L767
[45] Wu M C and Goodman D W 1994 *J. Phys. Chem.* **98** 9874
[46] Kaltchev M and Tysoe W T 1999 *Surf. Sci.* **430** 29
[47] Nagata K, Yamada C, Takahashi T and Murata Y 2003 *J. Phys.: Condens. Matter* **15** 8165
[48] Henrich V E and Cox P A 1994 *The Surface Science of Metal Oxides* (Cambridge: Cambridge University Press)
[49] He J W and Møller P J 1986 *Chem. Phys. Lett.* **129** 13
[50] Duriez C, Chapon C, Henry C R and Rickard J M 1990 *Surf. Sci.* **230** 123
[51] Duriez C, Chapon C, Henry C R and Rickard J 1990 *Surf. Sci.* **230** 123
[52] Giamello E, Paganini M C, Murphy D M, Ferrari A M and Pacchioni G 1997 *J. Phys. Chem.* B **101** 971
[53] Scorza E, Birkenheuer U and Pisani C 1997 *J. Chem. Phys.* **107** 9645
[54] Pacchioni G 2000 *Solid State Sci.* **2** 161
[55] Renaud G 1998 *Surf. Sci. Rep.* **32** 1
[56] Yuasa S, Nagahama T, Fukushima A, Suzuki Y and Ando K 2004 *Nat. Mater.* **3** 868
[57] Wu M C, Corneille J S, Estrada C A, He J-W and Goodman D W 1991 *Chem. Phys. Lett.* **182** 472
[58] He J-W, Estrada C A, Corneille J S, Wu M-C and Goodman D W 1992 *Surf. Sci.* **261** 164
[59] Wu M C, Estrada C A and Goodman D W 1991 *Phys. Rev. Lett.* **67** 2910
[60] Wu M C, Estrada C A, Corneille J S and Goodman D W 1992 *J. Chem. Phys.* **96** 3892
[61] He J-W, Corneille J S, Estrada C A, Wu M C and Goodman D W 1992 *J. Vac. Sci. Technol.* A **10** 2248
[62] Wu M C and Goodman D W 1992 *Catal. Lett.* **15** 1
[63] Wu M C, Truong C M, Coulter K and Goodman D W 1992 *J. Am. Chem. Soc.* **114** 7565
[64] Wu M C, Truong C M and Goodman D W 1992 *Phys. Rev.* B **46** 12688
[65] Wu M C, Truong C M, Coulter K and Goodman D W 1993 *J. Vac. Sci. Technol.* A **11** 2174
[66] Corneille J S, He J-W and Goodman D W 1994 *Surf. Sci.* **306** 269
[67] Xu X, Oh W S and Goodman D W 1996 *Langmuir* **12** 4877
[68] Gallagher M C, Fyfield M S, Cowin J P and Joyce S A 1995 *Surf. Sci.* **339** L909
[69] Gallagher M C, Fyfield M S and Joyce S A 1999 *Phys. Rev.* B **59** 2346
[70] Gallagher M C, Fyfield M S, Bumm L A, Cowin J P and Joyce S A 2003 *Thin Solid Films* **445** 90
[71] Gallagher M C, Fyfield1 M S, Cowin J P and Joyce S A 1995 *Surf. Sci.* **339** L909
[72] Benedettia S, Beniab H M, Niliusb N, Valeria S and Freund H J 2006 *Chem. Phys. Lett.* **430** 330
[73] Gunster J, Liu G, Kempter V and Goodman D W 1998 *Surf. Sci.* **415** 303
[74] Kolmakov A, Stultz J and Goodman D W 2000 *J. Chem. Phys.* **113** 7564
[75] Kim Y D, Stultz J, Wei T and Goodman D W 2002 *J. Phys. Chem.* B **106** 6827
[76] Kim Y D, Stultz J and Goodman D W 2002 *Langmuir* **18** 3999
[77] Kim Y D, Stultz J and Goodman D W 2002 *Surf. Sci.* **506** 228
[78] Yang Z X, Wu R Q, Zhang Q M and Goodman D W 2002 *Phys. Rev.* B **65** 155407
[79] Kim Y D, Stultz J, Wei T and Goodman D W 2003 *J. Phys. Chem.* B **107** 592
[80] Wendt S, Kim Y D and Goodman D W 2003 *Prog. Surf. Sci.* **74** 141
[81] Ochs D, Maus-Friedrichs W, Brause M, Günster J, Kempter V, Puchin V, Shluger A and Kantorovich L 1996 *Surf. Sci.* **365** 557
[82] Tegenkamp C, Pfnuer H, Ernst W, Malaske U, Wollschlaeger J, Peterka D, Schröder K M, Zielasek V and Henzler M 1999 *J. Phys.: Condens. Matter* **11** 9943
[83] Kramer J, Ernst W, Tegenkamp C and Pfnuer H 2002 *Surf. Sci.* **517** 87
[84] Sterrer M, Fischbach E, Risse T and Freund H-J 2005 *Phys. Rev. Lett.* **94** 186101
[85] Sterrer M, Fischbach E, Heyde M, Nilius N, Rust H-P, Risse T and Freund H J 2006 *J. Phys. Chem.* B **110** 8665
[86] Giovanardi C, di Bona A, Moia T S, Valeri S, Pisani C, Sgroi M and Busso M 2002 *Surf. Sci.* **505** L209
[87] Valeri S, Altieri S, del Pennino U, di Bona A, Luches P and Rota A 2002 *Phys. Rev.* B **65** 245410
Valeri S, Altieri S, del Pennino U, di Bona A, Luches P and Rota A 2002 *Surf. Sci.* **507** 311

[88] Schintke S, Messerli S, Pivetta M, Patthey F, Libioulle L, Stengel M, De Vita A and Schneider W-D 2001 *Phys. Rev. Lett.* **87** 276801
[89] Audibert P, Sidoumou M and Suzanne J 1992 *Surf. Sci.* **273** L467
[90] Gerlach R, Glebov A, Lange G, Toennies J P and Weiss H 1995 *Surf. Sci.* **331–333** 1490
[91] Heidberg J, Kandel M, Meine D and Wildt U 1995 *Surf. Sci.* **331–333** 1467
[92] Wichtendahl R, Rodrigez-Rodrigo M, Härtel U, Kuhlenbeck H and Freund H J 1999 *Phys. Status Solidi* a **173** 93
[93] Pacchioni G 2003 *ChemPhysChem* **4** 1041
[94] Poppa H 1983 *Ultramicroscopy* **11** 105
[95] Magkoev T T, Christmann K, Moutinho A M C and Murata Y 2002 *Surf. Sci.* **515** 538
[96] Vancampen D G and Hrbek J 1995 *J. Phys. Chem.* **99** 16389
[97] Lee S, Fan C Y, Wu T P and Anderson S L 2005 *J. Phys. Chem.* B **109** 11340
[98] He J W and Møller P J 1986 *Chem. Phys Lett.* **129** 13
[99] Giamello E, Paganini M C, Murphy D M, Ferrari A M and Pacchioni G 1997 *J. Phys. Chem.* B **101** 971
[100] Chiesa M, Paganini M C, Spoto G, Del Vitto A, Di Valentin C, Pacchioni G and Giamello E 2005 *J. Phys. Chem.* B **109** 7314
[101] Berger T, Sterrer M, Diwald O and Knoezinger E 2004 *J. Phys. Chem.* B **108** 7280
[102] Ferrari A M, Casassa S, Pisani C, Altieri S, Rota A and Valeri S 2005 *Surf. Sci.* **588** 160
[103] Kiguchi M, Goto T, Saiki K, Sasaki T, Iwasawa Y and Koma A 2002 *Surf. Sci.* **512** 97
[104] Luches P, D'Addato S, Valeri S, Groppo E, Prestipino C, Lamberti C and Boscherini F 2004 *Phys. Rev.* B **69** 045412
[105] Savio L, Celasco E, Vattuone L, Rocca M and Senet P 2003 *Phys. Rev.* B **67** 075420
[106] Purnell S K, Xu X, Goodman D W and Gates B C 1994 *J. Phys. Chem.* **98** 4076
[107] Purnell S K, Xu X, Goodman D W and Gates B C 1994 *Langmuir* **10** 3057
[108] Xue M S and Guo Q L 2007 *J. Phys. Chem.* **127** 054705
[109] Meyerheim H L, Popescu R, Kirschner J, Jedrecy N, Sauvage-Simkin M, Heinrich B and Pinchaux R 2001 *Phys. Rev. Lett.* **87** 076102
[110] Krischok S, Stracke P and Kempter V 2006 *Appl. Phys.* A **82** 167
[111] Xu X and Goodman D W 1992 *Appl. Phys. Lett.* **61** 774
[112] Xu X and Goodman D W 1993 *Surf. Sci.* **282** 323
[113] He J W, Xu X P, Corneille J S and Goodman D W 1992 *Surf. Sci.* **279** 119
[114] Schröder T, Adelt M, Richter B, Naschitzki M, Bäumer M and Freund H-J 2000 *Surf. Rev. Lett.* **7** 7
[115] Schröder T, Adelt M, Richter B, Naschitzki M, Bäumer M and Freund H J 2000 *Microelectron. Reliab.* **40** 841
[116] Schröder T, Hammoudeh A, Pykavy M, Magg N, Adelt M, Bäumer M and Freund H-J 2001 *Solid-State Electron.* **45** 1471
[117] Schröder T, Giorgi J, Bäumer M and Freund H-J 2002 *Phys. Rev.* B **66** 165422
[118] Chen M S, Santra A K and Goodman D W 2004 *Phys. Rev.* B **69** 155404
[119] Wendt S, Ozensoy E, Wei T, Frerichs M, Cai Y, Chen M S and Goodman D W 2005 *Phys. Rev.* B **72** 115409
[120] Chen M S and Goodman D W 2006 *Surf. Sci.* **600** L255
[121] Chen M S, Santra A K and Goodman D W 2004 *J. Phys. Chem.* B **108** 17940
[122] Yakovkin I N 2005 *Surf. Rev. Lett.* **12** 449
[123] Giordano L, Ricci D, Pacchioni G and Ugliengo P 2005 *Surf. Sci.* **584** 225
[124] Weissenrieder J, Kaya S, Lu J-L, Gao H-J, Shaikhutdinov S, Freund H-J, Sierka M, Todorova T K and Sauer J 2005 *Phys. Rev. Lett.* **95** 076103
[125] Todorova T K, Sierka M, Sauer J, Kaya S, Weissenrieder J, Lu J L, Gao H J, Shaikhutdinov S and Freund H J 2006 *Phys. Rev.* B **73** 165414
[126] Freysoldt C, Rinke P and Scheffler M 2007 *Phys. Rev. Lett.* **99** 086101
[127] Giordano L, Ricci D, Ricci D, Pacchioni G and Ugliengo P 2007 *Surf. Sci.* **601** 588
[128] Chen M S and Goodman D W 2007 *Surf. Sci.* **601** 591
[129] Queeney K T, Herbots N, Shaw J M, Atluri V and Chabal Y J 2004 *Appl. Phys. Lett.* **84** 493
[130] Sarnthein J, Pasquarello A and Car R 1997 *Science* **275** 1925
[131] Cornac M, Janin A and Lavalley J C 1986 *Polyhedron* **5** 183
[132] Kaya S, Baron M, Stacchiola D, Weissenrieder J, Shaikhutdinov S, Todorova T K, Sierka M, Sauer J and Freund H-J 2007 *Surf. Sci.* **601** 4849
[133] Wendt S, Frerichs M, Wei T, Chen M S, Kempter V and Goodman D W 2004 *Surf. Sci.* **565** 107
[134] Yates J T 2004 *Surf. Sci.* **565** 103
[135] Kim Y D, Wei T, Wendt S and Goodman D W 2003 *Langmuir* **19** 7929
[136] Kim Y D, Wei T and Goodman D W 2003 *Langmuir* **19** 354
[137] Diebold U 2003 *Surf. Sci. Rep.* **48** 53
[138] Chen M S and Goodman D W 2006 *Acc. Chem. Res.* **39** 739
[139] Oh W S, Xu C, Kim D Y and Goodman D W 1997 *J. Vac. Sci. Technol.* A **15** 1710
[140] Guo Q, Oh W S and Goodman D W 1999 *Surf. Sci.* **437** 49
[141] Lai X, Guo Q, Min B K and Goodman D W 2001 *Surf. Sci.* **487** 1
[142] Ashworth T V and Thornton G 2001 *Thin Solid Films* **400** 43
[143] Chang Z and Thornton G 2000 *Surf. Sci.* **462** 68
[144] McCavish N D and Bennett R A 2003 *Surf. Sci.* **546** 47
[145] Boffa A B, Galloway H C, Jacobs P W, Benitez J J, Batteas J D, Salmeron M, Bell A T and Somorjai G A 1995 *Surf. Sci.* **326** 80
[146] Sedona F, Rizzi G A, Agnoli S, Xamena F X L I, Papageorgiou A, Ostermann D, Sambi M, Finetti P, Schierbaum K and Granozzi G 2005 *J. Phys. Chem.* B **109** 24411
[147] Matsumoto T, Batzill M, Hsieh S and Koel B E 2004 *Surf. Sci.* **572** 127
Matsumoto T, Batzill M, Hsieh S and Koel B E 2004 *Surf. Sci.* **572** 146
[148] Chen M S and Goodman D W 2004 *Science* **306** 252
[149] Chen M S, Wallace W T, Kumar D, Zhen Y, Gath K K, Cai Y, Kuroda Y and Goodman D W 2005 *Surf. Sci.* **581** L115
[150] Kumar D, Chen M S and Goodman D W 2006 *Thin Solid films* **515** 1475
[151] Chen M S, Luo K, Yi C W and Goodman D W 2007 *Surf. Sci.* **601** 632
[152] Chen M, Cai Y, Yan Z and Goodman D W 2006 *J. Am. Chem. Soc.* **128** 6341
[153] Chen M S and Goodman D W 2007 *Top. Catal.* **44** 41–47
[154] Chen M S and Goodman D W 2006 *Acc. Chem. Res.* **39** 739
[155] Chen M S and Goodman D W 2006 *Catal. Today* **111** 22